Local structure of the Ag(100) surface reacting with molecular iodine: Experimental and theoretical study

B. V. Andryushechkin,* G. M. Zhidomirov, and K. N. Eltsov
A.M.Prokhorov General Physics Institute, Russian Academy of Sciences, Vavilov Str. 38, 119991 Moscow, Russia

Y. V. Hladchanka
A.M.Prokhorov General Physics Institute, Russian Academy of Sciences, Vavilov Str. 38, 119991 Moscow, Russia and Moscow Institute of Physics and Technology, Institutskii per. 9, 141700 Dolgoprudny, Moscow Region, Russia

A. A. Korlyukov
A.N.Nesmeyanov Institute of Organoelement Compounds, Russian Academy of Sciences, Vavilov Str. 28, 119991 Moscow, Russia
(Received 6 April 2009; revised manuscript received 14 July 2009; published 14 September 2009)

Room-temperature adsorption of molecular iodine on Ag(100) has been studied by scanning tunneling microscopy (STM), low-energy electron diffraction, Auger electron spectroscopy with factor analysis, and density-functional theory (DFT). We have found that at chemisorption stage iodine forms only one ordered phase c(2×2) described by a simple $(\sqrt{2}\times\sqrt{2})R45°$ unit cell. DFT calculations have shown that energetically most favorable configuration of this square lattice corresponds to iodine atoms adsorbed in fourfold hollow sites on the silver surface. Further iodine dosing leads to the growth of two-dimensional islands of silver iodide. The STM images of the silver-iodide surface demonstrate a clear visible superstructure with a periodicity $(2\sqrt{2}\times 12\sqrt{2})R45°$ superimposed with a quasihexagonal atomic modulation. As a result of the DFT simulations of the AgI islands, a new sandwichlike phase was obtained, which appears to be different from all known bulk structures of silver iodide. In the direction perpendicular to the sample face, it consists of two coupled silver planes located between two iodine planes. According to calculations, the "sandwich," as a whole, is situated on top of the c(2×2) iodine monolayer. The validity of the proposed structural model is confirmed by the excellent correspondence between experimental and simulated STM images.

DOI: 10.1103/PhysRevB.80.125409 PACS number(s): 68.43.Fg, 68.43.Bc, 68.47.Fg, 68.55.ag

I. INTRODUCTION

The interaction of halogens with silver or copper surfaces, known as a rather complicated process, gives rise to the formation of the chemisorbed monolayer of halogen atoms at the first stage of reaction and to the subsequent growth of metal halide film at the second one.[1,2] Halogens chemisorbed on the metal surface usually form a large variety of the ordered two-dimensional (2D) phases. This diversity arises from the competition between the lateral halogen-halogen interaction trying to pack atoms in the hexagonal lattice and the halogen-substrate interaction, which tends to impose to the adsorbate layer the symmetry and periodicity of the substrate. In particular, in the course of adsorption of halogens on (111) and (110) planes of silver and copper, one may observe both commensurate and incommensurate structures, with phase transitions between them following the domain-wall mechanism.[3–5]

For (100) surfaces of fcc metals characterized by the square symmetry, the corrugation of the surface potential is known to be much stronger in comparison with the case of (111) planes.[6] That is why, for most cases of adsorption of halogens on (100) planes of Ag and Cu, a simple commensurate structure c(2×2) was detected.[2] Only one exception corresponds to the case of iodine on Cu(100) (Ref. 7) since the lattice constant of the c(2×2) lattice (3.61 Å) (Ref. 8) appears to be much lower than van der Waals diameter of iodine (4.0–4.3 Å).[9–12] In this case, iodine forms a simple commensurate $p(2\times 2)$ lattice at 0.25 ML. Further coverage increase leads to a series of structural phase transitions and formation of a striped c(5×2) phase at monolayer saturation (0.4 ML).[7]

The detailed structural studies of thin halide films on metal surfaces have been performed for the systems exhibiting layer-by-layer growth: Br/Cu(100),[13] I/Cu(111),[14,15] I/Cu(100),[14,16] and I/Cu(110).[17] According to the scanning tunneling microscopy (STM) measurements, the lattice symmetry and interatomic distances on the surface of halide film in all cases appear to be close to ones for the hexagonal close-packed planes of corresponding bulk halides. For iodide on copper surfaces, it was found out that depending on the substrate symmetry, STM images of the CuI surface demonstrate different moiré-type patterns and striped misfit dislocation networks.[14–17] In the same works, the existence of the specific monatomic layer, playing a role of the interface between copper iodide and copper lattices, was evidently demonstrated. The structure of the interface appeared to be in a correspondence with a structure of saturated iodine monolayer forming at the first stage of reaction. It is also clear, that the detailed atomic structure of halide film cannot be unambiguously determined from the STM images. In particular, due to the proximity of the lattice parameters in the close-packed planes, it is not possible to distinguish between wurtzite and zinc-blende types of the crystalline lattice characteristic to the bulk CuBr and CuI.[8] Moreover, the structure of the inner layers of halide and their possible distortions due to the interaction with the substrate are also beyond of the direct interpretation of the STM images. In this connection,

the experimental STM information should be complemented by the theoretical structural calculations. The efficiency of such approach has been already shown on the example of surface oxides on transition metals, usually, as well as halides,[14–17] demonstrating the complex superstructures with large unit cells.[18] It was turned out, that the density-functional theory (DFT) calculations are capable to describe the structure of surface oxides in a good correspondence with the experimental data obtained with scanning tunneling microscopy and electron diffraction.[18]

Iodine adsorption on Ag(100) has been studied both experimentally[19–21] and theoretically.[22–24] In particular, formation of the $c(2\times2)$ monolayer at the initial stage of adsorption[19,20] and the hexagonal orientation of the growing silver-iodide film[19] were detected by low-energy electron diffraction (LEED). Teshima *et al.*[21] explored I/Ag(100) system in the electrochemical environment with STM. They confirmed the formation of the $c(2\times2)$ monolayer, observed faceting of the step edges during iodine adsorption but did not detect the growth of the silver-iodide film. Theoretical investigations of I/Ag(100) system were aimed at the determination of the preferable adsorption sites in the iodine monolayer. The fourfold hollow sites appear to be energetically more favorable, according to Ref. 24. Thus, there is a general agreement in the understanding of the iodine structure at the chemisorbed stage while the processes of the nucleation and the growth of AgI film on Ag(100) still need to be investigated.

In this paper, we present the results of iodine adsorption on the (100) face of silver. Using a combination of low-energy electron diffraction, Auger electron spectroscopy (AES) with factor analysis, scanning tunneling microscopy, and density-functional-theory calculations, we have determined the chemical state, morphology, and the detailed geometrical structure of the I/Ag(100) system starting from the stage of the chemisorbed iodine monolayer up to the formation of the thin silver-iodide film.

II. EXPERIMENTAL AND COMPUTATIONAL METHODS

A. Experimental setup and sample preparation

All the experiments were carried out in a UHV system consisting of two connected chambers. The first chamber, used for spectral analysis, was equipped with a cylindrical mirror analyzer (Riber OPC-200) for AES. The second chamber included a room-temperature STM (GPI-300, SigmaScan Ltd.) and 3-grid optics (VG RVL 640) for LEED measurements. A special transfer system moved samples and STM tips between the STM, AES, or LEED positions. The base pressure in both chambers did not exceed 1×10^{-10} Torr.

The silver sample was cut parallel to (100) plane with an accuracy better than 0.2°. To clean the surface, we used repetitive cycles of argon-ion bombardment (1 keV) and annealing at 800 K. As a result of such a treatment a sharp (1×1) LEED pattern and STM images with 600–1000 Å wide terraces were achieved. Auger spectra were acquired in the first derivative mode with modulation voltage of 1.8 V_{pp} and the current density of 80 $\mu A/cm^2$. The energy of the primary electron beam was 3 keV. Tungsten tips sharpened *in situ* by Ar^+ bombardment[25] were used for STM measurements. Iodine adsorption and STM measurements were carried out at room temperature. Molecular iodine was directly introduced on the sample face by means of a fine leak valve. To avoid possible contamination from residual gases in the chamber, the sample was cleaned and dosed again with iodine before each new STM measurement. The iodine coverage was calibrated by the intensity ratio (η) of I $M_{4,5}VV$ (495–540 eV) and Ag $M_{4,5}VV$ (335–365 eV) Auger peaks. For the treatment of the STM images, the freeware SPM software WSXM (Ref. 26) was used. To identify chemical states on a surface during iodination, we employ factor-analysis treatment of Auger spectra (AES-FA).[27,28] In Sec. II B, we present a short description of this method of data treatment.

B. Factor analysis of AES spectra

Factor analysis is a well-known statistical method that has been applied successfully in analytical chemistry.[27] Application of the factor analysis appeared to be useful when the total spectrum of the investigated system could be considered as a linear combination of the spectra of its components, with their concentrations being varied in the course of a process. It is important that the spectrum of the particular component be unique and independent of the component concentration in the system. Factor analysis allows both the number of independent components in the system to be determined and the behavior of each component to be determined separately. AES is considered to satisfy the requirements mentioned above. Factor analysis was introduced in AES by the pioneering work of Gaarenstroom[28] for depth profiling in thin films. To our knowledge, there are only a few papers in which factor analysis in Auger spectra has been applied to study the adsorption system, in particular, O/Ni,[29,30] Cl/Ag(111).[31]

A detailed formalism of factor analysis can be found in Ref. 27. In the first stage of factor analysis, the so-called principal-component analysis (PCA), the number of relevant factors (components) is obtained. The measured Auger spectra are written to the data matrix ($[D]$) as rows. Each of the rows of $[D]$ (m,n) consists of the signal intensities for the m points on the energy scale for the array of n spectra. The aim of the factor analysis is to break down the data matrix into a product of two matrices $[R]$ and $[C]$,

$$[D]=[R]\cdot[C], \tag{1}$$

where the matrix $[R]$ (m,c) contains Auger spectra of c pure components in the system and the matrix $[C]$ (c,n) contains the concentrations of each of c components in the array of n spectra.

According to Ref. 27, the number of independent components in the system c is equal to the number of the nonzero eigenvalues of a covariant matrix $[Z]=[D]^T[D]$. The indicator function[27] and the standard error in the eigenvalues (SE) (Ref. 32) are used to determine the number of the eigenvalues statistically different from zero. In the PCA stage, the pair of matrices ($[R^{\sim}]$ and $[C^{\sim}]$) could be obtained, satisfy-

ing condition (1). As a rule, the pair of matrices $[R^{\sim}]$ and $[C^{\sim}]$ is an abstract solution of Eq. (1) without any direct physical meaning. However, using the target transformation procedure, it is possible to obtain the required matrices $[R]$ and $[C]$. Formally, target transformation is a procedure for finding an appropriate matrix $[T]$ that will transform $[C^{\sim}]$ into $[C]$ and $[R^{\sim}]$ into $[R]$,[27]

$$[C] = [T] \cdot [C^{\sim}], \tag{2}$$

$$[R] = [R^{\sim}] \cdot [T]^{-1}. \tag{3}$$

To find the transformation matrix $[T]$, one should have information on the physical and chemical properties of the investigated system. The matrix $[T]$ can be obtained principally by two different test procedures ("target testing"). The procedure used more often is based on knowledge of the components in the system and their standard spectra. Spectra of the pure components form a standard matrix $[R^*]$, which also must satisfy Eq. (3). Mathematically, the least-square fitting of the matrix $[R^*]$ by the product $[R^{\sim}][T]^{-1}$ has to be performed for the calculation of the matrix $[T]$. Then, using Eq. (2), the matrix $[C]$, containing the concentration dependencies of the components, can be easily calculated. The second way to calculate $[T]$ is based on the knowledge or assumption of concentration dependencies. In this case, they form the matrix $[C^*]$, which should be fitted by the product $[T][C^{\sim}]$ according to Eq. (2). Finally, the calculation of the matrix $[R]$ is straightforward from Eq. (3).

C. Details of DFT calculations

All DFT calculations were carried out using the Vienna *ab initio* simulation package (VASP).[33–36] Exchange and correlation contributions into total energy were described by PW91 functional.[37] We used ultrasoft Vanderbilt-type pseudopotentials[38] as supplied by Kresse and Hafner.[39] The plane-wave cutoff energy of 350 eV is applied. With this setup a silver lattice constant (4.166 Å) was found to be in good agreement with the experimental value (4.085 Å).[8] For calculation of the atomic charge and the density of states, the radii of atomic spheres for iodine and silver were chosen 1.487 and 1.503 Å correspondingly. The substrate was modeled by three-, seven-, and nine-layer silver slabs. The vacuum region with a thickness of 15 Å was inserted between two neighboring slabs. To obtain accurate energy values the Kohn-Sham equations were integrated using Monkhorst-Pack (Ref. 40) k-point mesh $8\times8\times1$ [for the $(\sqrt{2}\times\sqrt{2})R45°$ unit cell] and $2\times1\times1$ [for the $(2\sqrt{2}\times12\sqrt{2})R45°$ unit cell]. Conjugated gradient technique was used for optimizations of the atomic positions and minimization of total energy. At a final step of our calculations, the forces on the atoms became smaller than 0.01 eV/Å.

The adsorption energy (per atom) was calculated as

$$E_{\mathrm{ads}} = \frac{1}{N_{\mathrm{I}}}\left[E_{\mathrm{Ag(100)+I}} - \left(E_{\mathrm{Ag(100)}} + \frac{1}{2}N_{\mathrm{I}} \cdot E_{\mathrm{I_2}}\right)\right], \tag{4}$$

where N_{I} is the number of adsorbed iodine atoms in the unit cell, $E_{\mathrm{Ag(100)+I}}$, $E_{\mathrm{Ag(100)}}$, and $E_{\mathrm{I_2}}$ are the total energies of the adsorbate system, the clean surface, and the free molecule I_2 in vacuum, respectively.

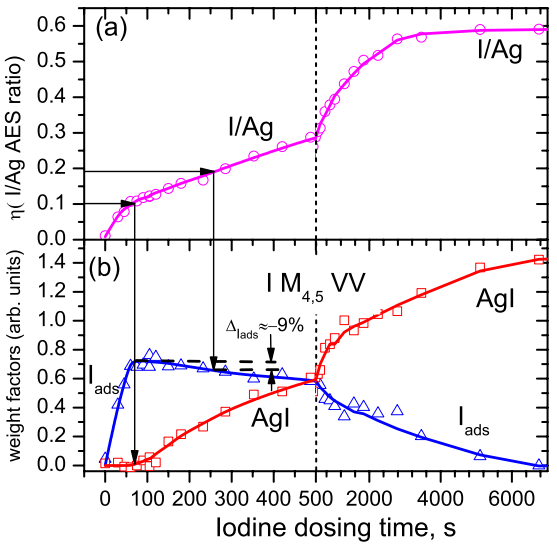

FIG. 1. (Color online) AES data obtained for molecular iodine adsorption on Ag(100) at room temperature. (a) Evolution of $I(M_{4,5}VV)/Ag(M_{4,5}VV)$ AES ratio (η) as a function of iodine dosing time [the local pressure of I_2 near the sample face was in the range of $(2\backslash5)\times10^{-8}$ Torr]; (b) Results of AES factor analysis performed for iodine $M_{4,5}VV$ Auger line. The behavior of AgI and I_{ads} components is indicated by squares and triangles correspondingly.

To compare the stability of the different AgI models on Ag(100), the surface formation energy was calculated as

$$E_{\mathrm{form}} = \frac{1}{A}\left[E_{\mathrm{Ag(100)+AgI}} - \left(E_{\mathrm{Ag(100)}} + N_{\mathrm{Ag}} \cdot E_{\mathrm{Ag}} + \frac{1}{2}N_{\mathrm{I}} \cdot E_{\mathrm{I_2}}\right)\right], \tag{5}$$

where N_{Ag} is the number of Ag atoms in the AgI layer, $E_{\mathrm{Ag(100)+AgI}}$ is the total energy of the adsorbate system with AgI, E_{Ag} is the total energy of a Ag atom in bulk fcc silver, and A is the surface area.

III. RESULTS AND DISCUSSION

A. Chemical state and morphology of Ag(100) in reaction with I_2

Figure 1 demonstrates the results of Auger measurements obtained for the step-by-step adsorption of molecular iodine on Ag(100). In Fig. 1(a) the I/Ag AES peak ratio (η) is shown as a function of dosing time (t). During iodine dosing, the pressure increment in the chamber was kept equal to 5×10^{-10} Torr, that approximately corresponds to the local pressure of I_2 near the sample surface in the range of $(2\backslash5)\times10^{-8}$ Torr. One can see that the rapid increase in η at the initial stage of adsorption is replaced by the more slowly changing growth on the second stage, reaching finally the saturation on the level of 0.59 [Fig. 1(a)]. The saturation of the curve in Fig. 1(a) corresponds to the formation of the multilayer film, with a thickness exceeding the escape depth of Auger electrons ($d>25$ Å). Although, the value of η does

TABLE I. The results of the principal-component analysis of the array of I $M_{4,5}VV$ Auger spectra.

I $M_{4,5}VV$	
λ[a]	SE[b]
92.597	0.1603
4.946	0.1378
0.034	0.1661
0.013	0.0984
0.012	0.1564
0.010	0.1473
0.009	0.1370

[a]λ eigenvalues of covariance matrix.
[b]SE in the eigenvalue (it is used to determine the number of eigenvalues statistically different from zero). Usually, the eigenvalue is considered to be nonzero if $\lambda > 2SE$ (Reference 32).

not provide any information on the chemical state of the surface, hereafter, we will use it as the indicator of the total amount of iodine atoms on the surface.

During adsorption, the position and the shape of silver and iodine Auger lines are subjected to significant changes induced by the chemical transformations of the surface. To follow the behavior of the different components during adsorption, we have applied Factor Analysis to the data matrix of the iodine $M_{4,5}VV$ spectral sequence. According to the theory [see Sec. II B], the number of independent components in the system is equal to the number of nonzero eigenvalues of the covariance matrix. Table I shows seven eigenvalues listed in the descending order together with SE in the eigenvalues.[27] Usually, to determine the number of the eigenvalues statistically different from zero, the criteria $\lambda > 2SE$ suggested by Hugus and El-Awady[32] is used. Thus, our system contains two relevant components, as follows from Table I. Their interpretation is straightforward: chemisorbed iodine and silver iodide. The normalized standard spectra of I_{ads} and AgI used in the factor-analysis scheme are shown in Fig. 2(a). As for the standard spectrum of I_{ads}, the iodine line at $t=45$ s was taken since according to PCA only one chemisorbed iodine component (I_{ads}) was detected at $t<70$ s. To obtain the standard spectrum of AgI, the additional five minute exposure of molecular iodine was made with the local pressure near the sample face about 1×10^{-7} Torr.

Figure 2(b) shows the result of the decomposition of iodine Auger line ($\eta=0.19$) into two components: I_{ads} and AgI. No doubts that experimentally measured Auger spectra can be reproduced by two-component fitting with a high accuracy.

Figure 1(b) demonstrate the behavior of different chemical components of iodine Auger line shown as functions of iodine dosing time. At the beginning of adsorption, the gradual increase in I_{ads} is detected. The onset of the silver iodide growth at $t\approx70$ s corresponds to the saturation point of the chemisorbed coverage at $\eta\approx0.10$. As iodine adsorbs, the intensity of the AgI component increases, coming to the saturation at $\eta=0.59$. In turn, at $t>70$ s, the intensity of the I_{ads} component drops gradually, reaching the zero level simultaneously with the saturation of the AgI signal.

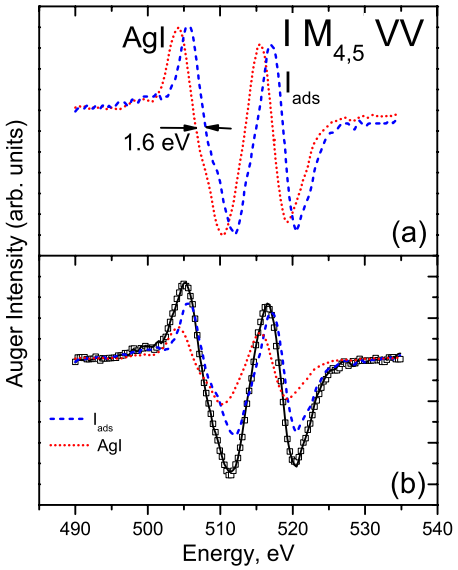

FIG. 2. (Color online) (a) Standard I $M_{4,5}VV$ spectra for chemisorbed iodine (dashed line) and silver iodide (dotted line). (b) Decomposition of I $M_{4,5}VV$ Auger line for $\eta=0.19$ into two components: I_{ads} (dashed line) and AgI (dotted line). Solid curve is a sum of dashed and dotted curves. The real experimental spectrum is shown by open squares.

Figure 3 shows the panoramic STM images of iodine on Ag(100) for the different values of η:0.12, 0.19, and 0.59. In addition to the flat terraces separated by the monatomic steps, the STM images in Fig. 3(a) demonstrate the 2D islands (visible as bright objects) situated mainly near the step edges. Since these islands were not detected below the saturation level of the chemisorbed monolayer ($\eta<0.10$), their identification as silver iodide is evident. If iodine is exposed further, the islands enlarge to fill the terraces while their height remains (≈4.5 Å) unchanged. At $\eta=0.19$ approximately a half of surface area is occupied by the AgI film, as shown in the STM frame in Fig. 3(b). Therefore, the 2D growth mode is realized at the initial stages of AgI formation.

Combining STM and factor-analysis data, the presence of the interface layer between the silver-iodide film and the substrate can be predicted. Indeed, the maximum of the I_{ads} intensity corresponds to $t\approx72$ s and $\eta=0.10$. At $\eta=0.19$, as shown in Fig. 1(b), iodine Auger line is a combination of two components: I_{ads} and AgI. At this moment, the dip of the I_{ads} curve with respect to the maximum is equal to 9%. From the other hand, according to the STM data in Fig. 3(b), the frac-

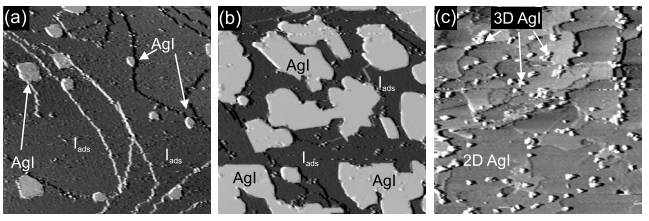

FIG. 3. [(a)–(c)] STM images (6000×6000 Å^2) showing the formation of AgI islands on Ag(100) for three different coverages characterized by η:0.12, 0.19, and 0.59.

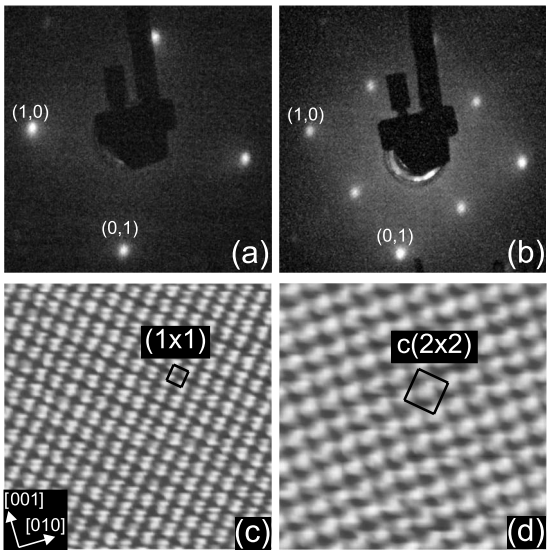

FIG. 4. LEED patterns (E_0=116 eV) of (a) clean Ag(100), (b) Ag(100)-c(2×2)-I. (c) STM image (46×46 Å^2, I_t=0.6 nA, U_s=−5 mV) showing the (1×1) periodicity of the clean Ag(100) substrate, (d) STM image (46×46 Å^2, I_t=0.2 nA, U_s=−360 mV) of the c(2×2) lattice of iodine at coverage 0.5 ML.

tion of the surface covered with chemisorbed iodine is very close to 50%. To find the cause of this discrepancy, the existence of the interface layer preserving the structure of chemisorbed monolayer has to be assumed. In this case, a little drop of the I_{ads} signal is naturally assigned to the screening effect by the AgI layer.

Figure 3(c) shows the STM image of a continuous multilayer AgI film (η=0.59). The appearance of the bright objects with a height of ≈35 Å on the step edges may be interpreted as the onset of the three-dimensional growth of silver iodide.

B. Atomic structure of Ag(100) in reaction with I_2

1. Monolayer of chemisorbed iodine

Figures 4(a) and 4(c) demonstrate the (1×1) LEED pattern and the atomic-resolution STM image of clean Ag(100). Figure 4(b) shows the c(2×2) LEED pattern observed for the saturated iodine monolayer on the Ag(100) surface. The STM image in Fig. 4(d) shows the atomic structure of the surface corresponding to the LEED pattern in Fig. 4(b). A perfect square structure with a lattice constant 4.1 Å is interpreted as a c(2×2) structure with one iodine atom per unit mesh. It is obvious that the coverage for this case is close to 0.5.

This result is predictable if one takes account of the previous diffraction data obtained in vacuum[19,20] and the STM electrochemical results.[21] To our knowledge, there are no published experimental data concerning the determination of iodine adsorption sites on Ag(100). Only one theoretical paper on this subject was presented by Wang *et al.*[24] In Ref. 24, the authors considered the $p(2\times2)$ iodine structure, never observed in the experiments.[19–21]

In the present paper, we have also examined iodine adsorption on Ag(100) with DFT. In our calculations, the experimentally detected c(2×2) structure with the $(\sqrt{2}\times\sqrt{2})R45°$ unit cell was investigated. Usually, adsorbed on the (100) surfaces of silver and copper, halogens do not form mixed layers.[2] In this connection, only three high-symmetry adsorption sites (see Fig. 5): fourfold hollow site, bridge site, and top site were considered.

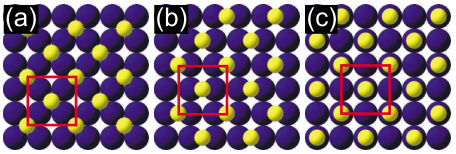

FIG. 5. (Color online) Models of the iodine c(2×2) monolayer on Ag(100) corresponding to the occupation of the fourfold (a) hollow sites, (b) bridge sites, and (c) top sites. Iodine and silver atoms are shown as small and large spheres, respectively.

The results of our DFT calculations are collected in Table II. The calculations of adsorption energies and positions of iodine atoms were performed for silver slabs containing three, seven, or nine atomic layers, with iodine adsorbed on the one side of the slab. Additionally, we present data for iodine adsorbed on the both sides of a nine-layer slab. As a result of calculations, it was established that energetically most favorable configuration of iodine atoms on Ag(100) surface corresponds to the occupation of the fourfold hollow sites. This conclusion is in line with results reported in Ref. 24 for the $p(2\times2)$ iodine structure.

It is noteworthy, that increase in the slab thickness from three to nine layers does not give rise to the appreciable

TABLE II. Structural and energetic properties of Ag(100)-c(2×2)-I. $N(N_{fixed})$—number of silver layers in the slab (number of the fixed layers). E_{ads}—adsorption energy, $r_\perp$—distance from I atom to the Ag(100) surface, and r_{NN}—distance from I atom to the nearest silver atom.

$N(N_{fixed})$	E_{ads} (eV/atom)	$r_\perp$ (Å)	r_{NN} (Å)
	Fourfold hollow site		
3 (1)	−1.420	2.112	2.966
7 (4)	−1.402	2.107	2.963
9 (4)	−1.430	2.109	2.964
9 (0)[a]	−1.386	2.108	2.963
	Top site		
3 (1)	−0.927	2.414	2.639
7 (4)	−0.884	2.441	2.639
9 (4)	−0.915	2.439	2.637
9 (0)[a]	−0.882	2.432	2.636
	Bridge site		
3 (1)	−1.203	2.324	2.772
7 (4)	−1.168	2.330	2.776
9 (4)	−1.200	2.322	2.772
9 (0)[a]	−1.158	2.328	2.775

[a]Iodine adsorption on the both sides of the slab.

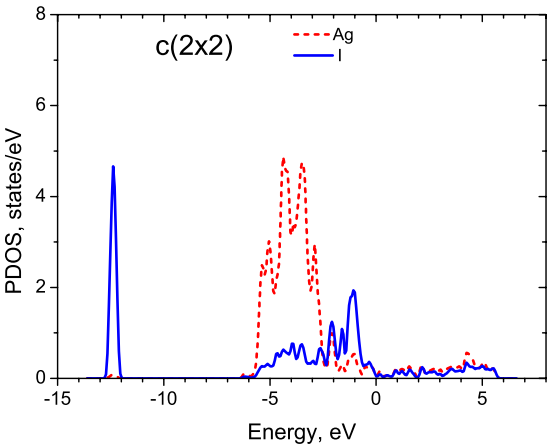

FIG. 6. (Color online) Density of states projected on iodine and silver atoms calculated for Ag(100)-c(2×2)-I structure, with iodine atoms adsorbed in the fourfold hollow sites. The energies are shown with respect to Fermi level.

changes in the system (for instance—switching energetically most favorable site to another position). Indeed, irrespective of the number layers in the slab, the difference in the adsorption energy between hollow, bridge, and top sites remains constant within ≈20 meV. In addition, the adsorbate atoms preserve their positions with accuracy better than 0.03 Å. Therefore, a three-layer slab seems to be enough for the adequate simulation of iodine adsorption on Ag(100).

Now we turn to analysis of chemical bonding between adsorbed halogen atom and the substrate. For many years the character of bonding of strongly electronegative halogens with metal surfaces was considered to be ionic. However, for some halogen/metal pairs, as shown in the recent publications by Migani *et al.*[23] and Baker *et al.*,[41] the character of interaction is much more close to covalent than to ionic. In particular, such a conclusion was made for Cl/Au(111) system[41] characterized by the difference in Pauling electronegativity between Au and Cl of 0.76. For our system, the difference in the electronegativity between iodine and silver is equal to 0.73 (Ref. 42) that can indicate the covalent character of interaction. We have calculated, that iodine atom adsorbed on silver surface gains additional charge equal to $-0.18|e|$ ($-0.29|e|$ in Ref. 23) in comparison with free atom in vacuum. According to Migani *et al.*[23] the charge transfer lower than $-0.3|e|$ indicates the covalent bonding. Additional evidence in this favor can be found in partial density of states (PDOS) curves calculated for iodine and silver states (see Fig. 6). The clearly seen mixing of iodine and silver states both in occupied and unoccupied part indicates the covalent bonding.

2. Silver-iodide film

Figure 7(a) demonstrates an atomic-resolution STM image of the silver-iodide island. The atomic structure roughly corresponds to the hexagonal lattice, as shown in the inset. The STM image of AgI, in addition to atomic modulation, contains the clearly seen superstructure with the periods of 52 and 8 Å, as measured along the [001] and [010] directions, respectively.

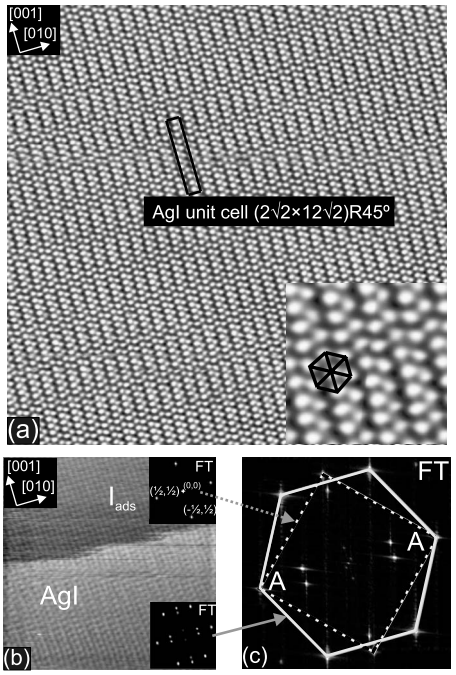

FIG. 7. (a) An atomic-resolution STM image (277×277 Å^2, I_t=0.23 nA, U_s=−250 mV) of the AgI surface. In the inset a nearly hexagonal lattice of AgI is indicated by the hexagon. (b) The STM image (159×159 Å^2, I_t=0.2 nA, U_s=−250 mV), demonstrating the edge of the AgI island and the atomic terrace with the c(2×2) iodine monolayer. The inset in the upper right corner shows the FT image of the monolayer region while the inset in the lower right corner the FT image of AgI. (c) The superimposition of the Fourier transformation images for the c(2×2) monolayer and AgI.

The STM image shown in Fig. 7(b) contains areas covered with both silver-iodide and chemisorbed iodine monolayer. Taking account of the known lattice parameters for iodine monolayer, it is possible to determine the parameters of silver-iodide lattice from this image. The saturated monolayer of chemisorbed iodine is described by a simple square lattice with I-I nearest-neighbor distance of 4.09 Å. Analysis of the STM image shows that one of the directions of the close-packed AgI atomic rows is parallel to the close-packed atomic row of the chemisorbed monolayer, and, accordingly, to the [001] direction of the substrate. The accurate reconstruction of the silver-iodide lattice was done on the basis of analysis of the Fourier transformation (FT) image. The FT image of silver-iodide lattice [see the bottom inset in Fig. 7(b)] contains six main bright spots arranged in a slightly distorted hexagon. Additional four pairs of spots in the FT image are associated with visible superstructure in the STM image. The FT image of chemisorbed monolayer, according to the upper insert in Fig. 7(b), contains a square of four spots corresponding to the known c(2×2) structure. In Fig. 7(c) the superposition of the FT images of AgI and chemisorbed iodine is presented. The hexagon and the square intersect in two points marked as "A." This observation means a full coincidence of the distances between atomic rows of AgI and chemisorbed iodine in the [010] direction (4.09 Å). As a sequence, we have found that the upper plane of silver

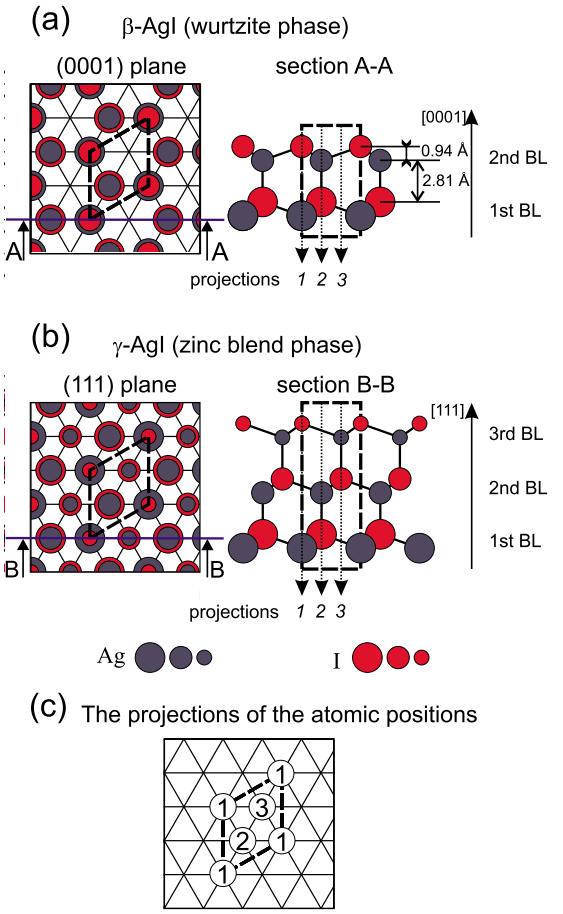

FIG. 8. (Color online) Atomic structure of AgI: (a) β-AgI; (b) γ-AgI; (c) The definition of positions y (1, 2, 3), used to identify the projections of the atomic positions. Dashed line indicates the irreducible cell.

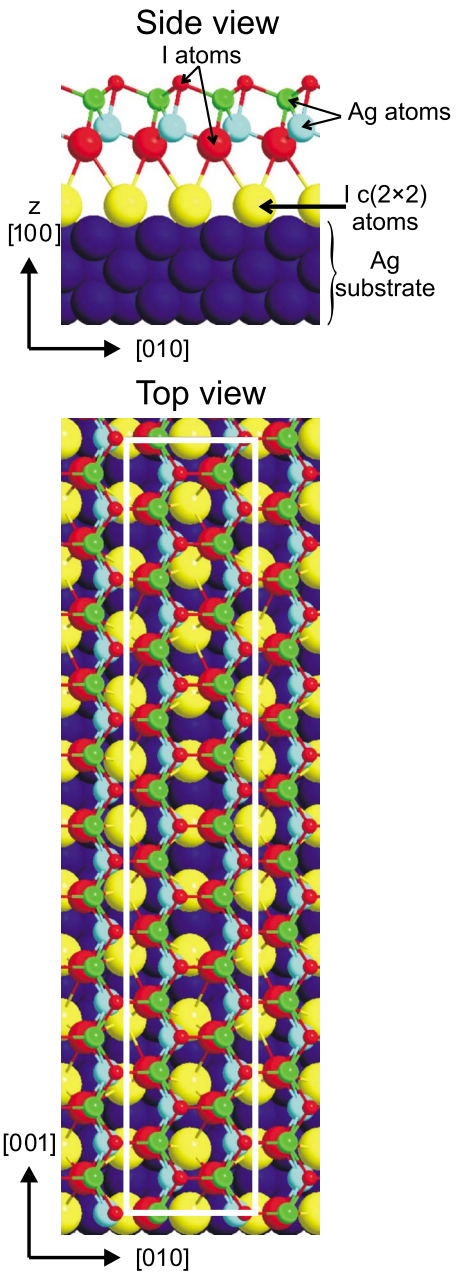

FIG. 9. (Color online) The sandwichlike model of the AgI film obtained as a result of the DFT calculations.

iodide is described by a slightly compressed quasihexagonal lattice with average parameters 4.33, 4.62, and 4.62 Å. Additionally, from the FT image in Fig. 7(c) the unit cell of the superstructure was determined as $(2\sqrt{2}\times p\sqrt{2})R45°$, $p \approx 12.0 \pm 0.5$.

Now we turn to the theoretical DFT analysis of silver-iodide islands on Ag(100). The atomic structure of silver iodide deserves special attention. At normal conditions AgI crystallizes not only in β (wurtzite) phase [a=4.580 Å and c=7.494 Å (Ref. 8) but also in γ (zinc-blende) phase [a=6.473 Å (Ref. 8]. Wurtzite phase in the direction ⟨0001⟩ and zinc-blende phase in the direction ⟨111⟩ consist of the sequences of alternate hexagonal Ag-I bilayers. The irreducible cell for β-AgI and γ-AgI contains two and three bilayers, respectively [see Figs. 8(a) and 8(b)]. Note that, the distances between silver and iodine planes in one bilayer (0.94 Å) and the distances between bilayers (2.81 Å) are identical within 0.01 Å for the both β and γ phases. There is also a close agreement between the lattice parameters in the (0001) plane of the β phase and in the (111) plane of the γ phase (4.580 versus 4.577 Å).[8]

The projections of all atom positions onto the (111) plane for β-AgI and onto the (0001) plane for γ-AgI may be distributed among three positions (y): 1, 2, and 3, as shown in Fig. 8(c). To identify the hexagonal layer of X(I or Ag) atoms occupying the position y, the notation X^y can be used. The structure of β-AgI, therefore, may be rewritten as $-(Ag^1I^2\text{-}Ag^2I^1)-\ldots$. In fact, this expression means that the irreducible cell consists of two Ag-I bilayers. In addition, in the first bilayer, the positions of silver atoms correspond to 1 and the positions of iodine atoms to 2. In the second bilayer, silver atoms occupy positions 2 and iodine atoms −1. In the notation, the dash shows the transition from one bilayer to another. In these terms, the structure of the γ-AgI phase looks as $-(Ag^1I^2\text{-}Ag^2I^3\text{-}Ag^3I^1)-\ldots)-\ldots$

Since the structure and the sequence of layers in the thin island film may be different from ones in the bulk AgI crystal, the number of the Ag-I bilayers and their positional re-

TABLE III. The structural models of silver iodide explored with DFT. Surface formation energies (E_{form}) are listed.

Model	Presence of the c(2×2) layer	Initial configuration	E_{form}, eV
		2 bilayers	
A	yes	Ag(100)-$I_{c(2\times2)}$-Ag^1I^2-Ag^2I^1 (β-AgI like)	−2.81
B	yes	Ag(100)-$I_{c(2\times2)}$-Ag^1I^2-Ag^2I^3 (γ-AgI like)	−2.65
C	yes	Ag(100)-$I_{c(2\times2)}$-Ag^1-I^1Ag^2-I^2	−2.05
D	no	Ag(100)-Ag^1I^2-Ag^2I^1 (β-AgI like)	−1.72
E	no	Ag(100)-Ag^1I^2-Ag^2I^3 (γ-AgI like)	−1.68
F	no	Ag(100)-Ag^1-I^1Ag^2-I^2	−1.05
		1.5 bilayers	
G	yes	Ag(100)-$I_{c(2\times2)}$-I^1-Ag^1I^2	−2.03
H	yes	Ag(100)-$I_{c(2\times2)}$-I^1Ag^2-I^2	−2.19
I	no	Ag(100)-I^1-Ag^1I^2	−1.87
J	no	Ag(100)-I^1Ag^2-I^2	
		1 bilayer	
K	yes	Ag(100)-$I_{c(2\times2)}$-Ag^1I^2	−2.01

lationship in the initial model for the DFT calculations are of the great importance. As measured in the STM images from Figs. 3(a) and 3(b), the height of the islands ranges from 4.0 to 4.5 Å depending on the bias voltage. This value, strictly speaking, does not inform on the real height due to the obvious differences in the electronic structure of silver iodide and chemisorbed iodine. In addition, the height of the islands measured in the STM images for the thin films of isolators or wide-gap semiconductors, such as AgI, is known to be systematically underestimated.[43] Further information on the real height of the islands may be extracted from the STM image of the multilayer silver-iodide film [Fig. 3(c)]. The minimum step height appears to be equal to ≈7.5 Å in a good correspondence with a thickness of the two-bilayer film.[8] As a sequence of this observation, the two-bilayer increment of the film thickness on each stage of the film growth is expected. Therefore, it is reasonable to assume that the silver-iodide islands formed at the first stage of the growth also consist of two bilayers. This remark allowed reducing the number of models in our consideration.

To explain the superstructure in the STM images, the substrate and the possible interface layer have to be included in the models in addition to the silver-iodide layer. To describe the substrate, a three-layer silver slab has been used (see the final remark in Sec. III B 1). As the interface, we have chosen the c(2×2) iodine monolayer, which, according to factor-analysis data, remains between the silver-iodide layer and the substrate. In the starting models, the silver-iodide lattice has been slightly compressed to correspond the $(2\sqrt{2}\times12\sqrt{2})R45°$ unit cell, as determined from the STM in Fig. 7.

We investigated a number of different initial configurations (A-K) listed in Table III. To identify the configurations, the notations taken from Fig. 8 were used. Models consisting of one, one and a half, and two Ag-I bilayers in the different combinations placed on both the c(2×2) interface iodine layer and clean Ag(100) have been explored. It is noteworthy that all configurations presented in Table III correspond to iodine termination of silver iodide.

The optimization of coordinates performed for the model A [two bilayers in wurtzite structure on top of the c(2×2) monolayer] gives rise to the significant modification of the initial configuration—flipping of the lower bilayer. As a result, a sandwichlike structure is formed. The sandwich is formed by two coupled silver layers in the middle and two layers of iodine on the borders (Fig. 9). All four atomic layers of the sandwich are very close to the ideal planes since the deviations of the atomic coordinates along the z axis ([100] direction of the substrate) for both iodine and silver layers does not exceed 0.1 Å. The atomic structure of each layer of the sandwich is described by the quasihexagonal lattice. The close-packed atomic rows parallel to the [001] direction of the substrate also remain straight within 0.1 Å.

During optimization of the initial configurations B, I, and K, the atomic layers remain flat within 0.6 Å. No modification of the sequence of the atomic layers along the z direction is detected in this case. The optimization of the initial configurations C, D, E, F, G, and H leads to significant (more than 1 Å) bending of atomic layers and to the disorder of the atomic structure that is not in line with the experimental STM observations. The optimization of the model J gives rise to the rapid lost of the ordering in the upper layers and to the structural instability.

Note, that the silver-terminated trial models of AgI film have been also tested. They differ from discussed above models A-K by the inverted sequence of Ag and I atomic layers. For the most of the considered Ag-terminated models, the optimization resulted in the disordering of atomic structure. All disordered final structures appeared to be energetically less favorable than models A-I and K. There are, how-

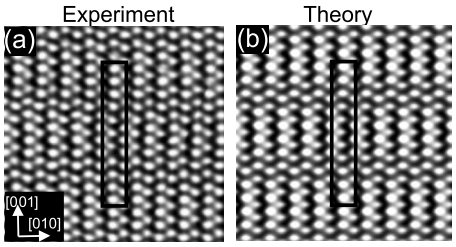

FIG. 10. (a) The fragment of the experimental STM image of the AgI surface (U_s=−260 meV), (b) STM image simulated for the sandwichlike model of the AgI film.

ever, two exceptions: Ag(100)-$I_{c2\times2}$-I^1Ag^2-I^2Ag^1 [two bilayers in wurtzite structure placed on top of the c(2×2) monolayer] and Ag(100)-$I_{c2\times2}$-I^1Ag^2 [one bilayer on top of the c(2×2) monolayer]. For the first starting configuration, the upper silver layer moved down below the upper iodine layer forming the sandwichlike structure similar to the case of the model A. For the second configuration, the interchange of iodine and silver layers was obtained. As a result the structure came to the model K.

It should be also noticed that for all considered initial configurations, containing the interface iodine layer, the distortion of its c(2×2) lattice was negligible.

The formation energies for all explored configurations are presented in Table III. The sandwichlike structure appears to be the most stable. To confirm this structure, we have compared the experimental and calculated STM images. The Tersoff-Hamann approach[44] was applied to simulate STM images from the *ab initio* calculation. The STM image was approximated by the charge density integrated between −0.4 and 0 eV. The STM images were calculated for all optimized configurations listed in Table III. The best agreement of the simulated STM image with experimental one was achieved for the sandwichlike structure, as shown in Fig. 10. Indeed, the theoretical image reproduces all characteristic features observed in the experiment. Note also, that the visible coupling of the atomic rows in the STM images is due to the electronic effect since the real atomic positions are not modulated.

The nature of the chemical bonding in AgI is also of the great interest. According to the literature,[45–47] the covalent bonding in bulk AgI is important. We have calculated the charge on iodine atom and PDOS curves for the sandwichlike structure. According to our findings, iodine atom in the sandwich gains additional charge $-0.19|e|$ in comparison with free atom in vacuum. PDOS plots in Fig. 11 show the mixing of silver and iodine states. As in the case of monolayer, these two factors indicate the important contribution of covalent bonding in the stabilizing of the sandwich. Thus, the electrostatic interaction seems not to play the dominant role in our system.

IV. CONCLUSIONS

Thus, the interaction of molecular iodine with Ag(100) at 300 K has been studied with STM, LEED, AES-FA, and DFT techniques. At the first stage of adsorption, iodine forms

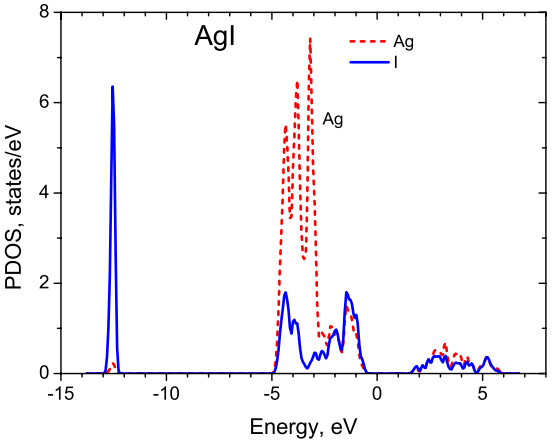

FIG. 11. (Color online) Density of states projected on iodine and silver atoms calculated for the sandwichlike silver-iodide structure. The energies are shown with respect to Fermi level.

a simple monolayer with a c(2×2) structure. The DFT calculations indicated that iodine preferably occupies the fourfold hollow adsorption sites. After saturation of the chemisorbed layer, the nucleation and growth of the flat silver-iodide islands start near the step edges. According to the DFT calculations, the silver-iodide islands are consisted of four hexagonal atomic planes parallel to the substrate surface. They are arranged in the sandwichlike structure, containing two coupled silver planes in the middle and iodine planes on each side. The sandwich as a whole is situated on top of the c(2×2) iodine monolayer which remains as the atomically sharp interface between AgI and the substrate.

The first noteworthy result of the work concerns existence of the interface layer between the halide film and the substrate. We have evidently demonstrated that the saturated iodine monolayer does remain under the halide film as the atomically sharp interface. This result seems to be common, since, according to the previous studies, the explanation of the superstructures detected in the STM images of CuI films grown on copper single-crystal surfaces became possible only with taking into account the interface preserving the structure of saturated monolayer.[14,17]

We have also found that for the AgI/Ag(100) system the halide layer appears to be separated from the substrate. Indeed, the distances between iodine atoms from the interface and iodine atoms from the sandwich are close to ≈4 Å in a good correspondence with iodine van der Waals diameter [4.0–4.3 Å (Ref. 9–12)]. This observation is in line with our conclusions on the covalent character of bonding for both the (2×2) and silver-iodide layers. It is likely that this "independence" of halide layer from the underlying substrate can explain, why during the halide growth on the fcc metals, independently of the substrate symmetry, the upper halide planes correspond to the hexagonal close-packed lattice.[13–17,19,48–50]

ACKNOWLEDGMENTS

This work was supported in part by the grants of the Russian Foundation for Basic Research under Grants No. 08-02-

01456-a and No. 05-02-22004-a-CNRS. We thank the Chair of informatics of Moscow Institute of Physics and Technology for provision of computational facilities on MIPT-60 high performance computing system. We would like to thank A. V. Nikolaev for helpful conversations and technical assistance in the course of our work with MIPT-60. We are also grateful to Laboratory for X-ray Diffraction Studies of A. N. Nesmeyanov Institute of Organoelement Compounds Russian Academy of Sciences for support on the early stages of our computational work.

*andrush@kapella.gpi.ru

[1] R. G. Jones, Prog. Surf. Sci. **27**, 25 (1988).
[2] E. I. Altman, in *Physics of Covered Solid Surfaces: Part I. Adsorbed Layers on Surfaces*, edited by H. P. Bonzel (Springer-Verlag, Berlin, 2001).
[3] B. V. Andryushechkin, K. N. Eltsov, and V. M. Shevlyuga, Surf. Sci. **470**, L63 (2000).
[4] B. V. Andryushechkin, K. N. Eltsov, and V. M. Shevlyuga, Surf. Sci. **472**, 80 (2001).
[5] B. V. Andryushechkin, K. N. Eltsov, and V. M. Shevlyuga, Surf. Sci. **584**, 278 (2005).
[6] A. Patrykiejew, S. Sokolowski, and K. Binder, Surf. Sci. Rep. **37**, 207 (2000).
[7] B. V. Andryushechkin, K. N. Eltsov, V. M. Shevlyuga, U. Bardi, and B. Cortigiani, Surf. Sci. **497**, 59 (2002).
[8] R. W. G. Wyckoff, *Crystal Structures*, 2nd ed. (John Wiley & Sons, New York, 1963).
[9] A. Bondi, J. Phys. Chem. **68**, 441 (1964).
[10] A. Gavezzotti, J. Am. Chem. Soc. **105**, 5220 (1983).
[11] P. Chauvin, J. Phys. Chem. **96**, 9194 (1992).
[12] R. S. Rowland and R. Taylor, J. Phys. Chem. **100**, 7384 (1996).
[13] C. Y. Nakakura and E. I. Altman, Surf. Sci. **424**, 244 (1999).
[14] B. V. Andryushechkin, K. N. Eltsov, and V. M. Shevlyuga, Surf. Sci. **566-568**, 203 (2004).
[15] N. T. M. Hai, S. Huemann, R. Hunger, W. Jaegermann, K. Wandelt, and P. Broekmann, J. Phys. Chem. C **111**, 14768 (2007).
[16] P. Broekmann, N. T. M. Hai, and K. Wandelt, J. Appl. Electrochem. **36**, 1241 (2006).
[17] B. V. Andryushechkin, K. N. Eltsov, and V. V. Cherkez, JETP Lett. **83**, 162 (2006).
[18] E. Lundgren, A. Mikkelsen, J. N. Andersen, G. Kresse, M. Schmid, and P. Varga, J. Phys.: Condens. Matter **18**, R481 (2006).
[19] U. Bardi and G. Rovida, Surf. Sci. **128**, 145 (1983).
[20] K. K. Kleinherbers, E. Janssen, A. Goldmann, and H. Saalfeld, Surf. Sci. **215**, 394 (1989).
[21] T. Teshima, K. Ogaki, and K. Itaya, J. Phys. Chem. B **101**, 2046 (1997).
[22] A. Ignaczak and J. A. N. F. Gomes, J. Electroanal. Chem. **420**, 71 (1997).
[23] A. Migani and F. Illas, J. Phys. Chem. B **110**, 11894 (2006).
[24] Y. Wang, W. Wang, K. Fan, and J. Deng, Surf. Sci. **487**, 77 (2001).
[25] K. N. Eltsov, V. M. Shevlyuga, V. Yu. Yurov, A. V. Kvit, and M. S. Kogan, Phys. Low-Dimens. Semicond. Struct. **9**, 7 (1996).
[26] I. Horcas, R. Fernandez, J. M. Gomez-Rodriguez, J. Colchero, J. Gomez-Herrero, and A. M. Baro, Rev. Sci. Instrum. **78**, 013705 (2007).
[27] E. R. Malinowski and D. G. Howery, *Factor Analysis in Chemistry* (Wiley, New York, 1980).
[28] S. W. Gaarenstroom, J. Vac. Sci. Technol. **20**, 458 (1982).
[29] J. Steffen and S. Hofmann, Surf. Sci. **202**, L607 (1988).
[30] S. Hofmann and J. Steffen, Surf. Interface Anal. **14**, 59 (1989).
[31] B. V. Andryushechkin, K. N. Eltsov, V. M. Shevlyuga, and V. Y. Yurov, Surf. Sci. **431**, 96 (1999).
[32] A. A. El-Awady and Z. Z. Hugus, J. Phys. Chem. **75**, 2954 (1971).
[33] G. Kresse and J. Hafner, Phys. Rev. B **47**, 558 (1993).
[34] G. Kresse and J. Hafner, Phys. Rev. B **49**, 14251 (1994).
[35] G. Kresse and J. Furthmuller, Comput. Mater. Sci. **6**, 15 (1996).
[36] G. Kresse and J. Furthmuller, Phys. Rev. B **54**, 11169 (1996).
[37] J. P. Perdew, J. A. Chevary, S. H. Vosko, K. A. Jackson, M. R. Pederson, D. J. Singh, and C. Fiolhais, Phys. Rev. B **46**, 6671 (1992).
[38] D. Vanderbilt, Phys. Rev. B **41**, 7892 (1990).
[39] G. Kresse and J. Hafner, J. Phys. Condens. Matter **6**, 8245 (1994).
[40] H. J. Monkhorst and J. D. Pack, Phys. Rev. B **13**, 5188 (1976).
[41] T. A. Baker, C. M. Friend, and E. Kaxiras, J. Am. Chem. Soc. **130**, 3720 (2008).
[42] http://www.webelements.com
[43] W. Hebenstreit, J. Redinger, Z. Horozova, M. Schmid, R. Podloucky, and P. Varga, Surf. Sci. **424**, L321 (1999).
[44] J. Tersoff and D. R. Hamann, Phys. Rev. B **31**, 805 (1985).
[45] H. Takahashi, S. Tamaki, and S. Sato, J. Phys. Soc. Jpn. **56**, 1773 (1987).
[46] N. Shimoji, T. Tomoyose, H. Watanabe, and M. Kobayashi, Ionics **12**, 275 (2006).
[47] M. Kobayashi, in *Physics of Solid State Ionics*, edited by T. Sakuma and H. Takahashi (Research Signpost, Kerala, 2006), pp. 1–15.
[48] M. Galeotti, B. Cortigiani, M. Torrini, U. Bardi, B. Andryushechkin, A. Klimov, and K. Eltsov, Surf. Sci. **349**, L164 (1996).
[49] B. V. Andryushechkin, K. N. Eltsov, and V. M. Shevlyuga, Surf. Sci. **433-435**, 109 (1999).
[50] B. V. Andryushechkin, K. N. Eltsov, V. M. Shevlyuga, C. Tarducci, B. Cortigiani, U. Bardi, and A. Atrei, Surf. Sci. **421**, 27 (1999).